

Folding Transitions of the Square-Diagonal Lattice

P. Di Francesco*,

*Department of Mathematics,
University of North Carolina at Chapel Hill,
CHAPEL HILL, N.C. 27599-3250, U.S.A.*

We address the problem of "phantom" folding of the tethered membrane modelled by the two-dimensional square lattice, with bonds on the edges and diagonals of each face. Introducing bending rigidities K_1 and K_2 for respectively long and short bonds, we derive the complete phase diagram of the model, using transfer matrix calculations. The latter displays two transition curves, one corresponding to a first order (ferromagnetic) folding transition, and the other to a continuous (anti-ferromagnetic) unfolding transition.

* e-mail: philippe@math.unc.edu

1. Introduction

Models for discrete polymerized membranes with rigid bonds display interesting physical behaviors, as the only way to change their spatial configuration is through folding. We will consider here only "phantom" folding, in which the membrane is allowed to interpenetrate itself, as opposed to self-avoiding folding, which introduces considerable mathematical difficulties, as was already noticed in the case of compact (one-dimensional) polymer folding [1].

The entropy of folding of a regular triangular lattice has been first studied numerically in [2] and later computed exactly in [3], by mapping the model onto the edge tri-coloring problem of the triangular lattice. The next step was the introduction of a bending rigidity, namely an energy which favors either folded edge states or unfolded ones (typically, one associates the Boltzmann weights $e^{\pm K}$ respectively to each unfolded or folded edge). Numerical studies [4] have shown the existence of a first order folding transition between completely folded states (with a certain entropy) and a unique completely flat state, at a critical value $K = K_c > 0$. On the other hand, the model also displays a continuous unfolding transition between a completely folded state and a partially unfolded one at another critical value $K = K_* < 0$. Only little numerical evidence for the latter transition was found in [4], but it was argued that for $K < 0$, starting from a completely folded state, edges could be unfolded along loops, a phenomenon typical of continuous (Ising-like) transitions.

In the present paper, we carry out an analogous study for the square-diagonal lattice folding problem introduced in [5]. The square-diagonal lattice (see Fig.1 below) has two types of edges, long and short, it is therefore natural to attach to them two different types of Boltzmann weights, $e^{\pm K_i}$, $i = 1, 2$ for respectively short and long edges. In addition to getting better numerical estimates when $K_2 = 0$ or $K_1 = 0$, we will be able to investigate the full critical structure of the model in the plane (K_1, K_2) .

The paper is organized as follows. In Sect.2, we review the 2-dimensional folding problem of the square-diagonal lattice, and its reformulation as an edge tangent-vector model, and various face/vertex models. In the presence of bending rigidity, the transfer matrix of the model is simple enough to permit numerical estimates of the free energy and magnetization, by extraction of its largest eigenvalue. Sect.3 is devoted to the numerical study of the rigid short edge model, with $K_2 = 0$, in which only the short edges have a bending rigidity, whereas Sect.4 deals with the rigid long edge model, with $K_1 = 0$. Both

models confirm the first order folding transition of [4], at some critical values $K = K_{c,i} > 0$. In Sect.5, the two above models are studied for $K_i < 0$, and better evidence is found for a continuous unfolding transition at some critical values $K_i = K_{i,*} < 0$. The general rigid long and short edge model is studied in Sect.6, where we find the complete phase diagram of the model, including two critical curves corresponding to the folding and unfolding transitions, and which are separated by the line $K_2 = -2K_1$.

2. Folding the Square-Diagonal Lattice

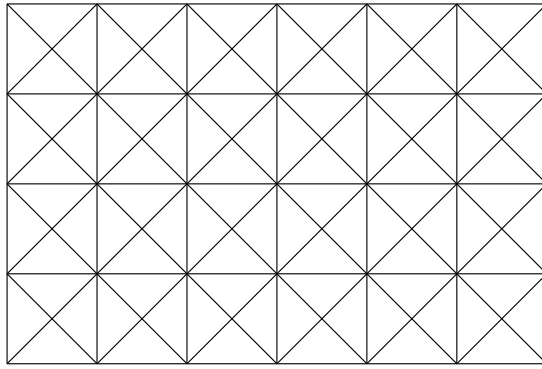


Fig. 1: The Square-Diagonal lattice. It has two types of vertices, respectively 4- and 8-valent, and two types of edges, short (length 1) and long (length $\sqrt{2}$).

Let us consider the *Square-Diagonal lattice*, obtained from the standard square lattice by drawing the two diagonals on each face, as depicted in Fig.1. Each face of this lattice is a triangle with two "short" edges of length 1 and one "long" edge of length $\sqrt{2}$. In this paper we study the possible foldings of the lattice, in which the edges serve as hinges between adjacent faces. The simplest such foldings are those with a two-dimensional final state, namely the foldings of the lattice into itself. Here we consider only *phantom* folding, in which the lattice may interpenetrate itself, and distinguish only between distinct final two-dimensional (folded) states of the lattice, namely its *folding configurations*.

In [4], we have shown that this two-dimensional folding problem is equivalent to various vertex models. We first defined the tangent vectors to the lattice as the vectors \vec{t} drawn along its edges, oriented in a compatible way, so that the sum

$$\sum_{\text{face}} \vec{t} = \vec{0} \quad (2.1)$$

taken around each face of the lattice vanishes. The short tangent vectors may take the 4 values $\pm\vec{e}_1, \pm\vec{e}_2$, where (\vec{e}_1, \vec{e}_2) is an orthonormal basis for the short edges, whereas the long edges may take the 4 values $\pm\vec{e}_1 \pm \vec{e}_2$.

A folding configuration of the lattice is entirely determined by the images of these tangent vectors under a continuous, length-preserving folding map ρ , with the constraint

$$\sum_{\text{face}} \rho(\vec{t}) = \vec{0} \quad (2.2)$$

around each face of the lattice. Note that the images of the tangent vectors under ρ may take only values in the corresponding abovementioned sets of 4.

By focusing on either short or long edges (the images of either class are sufficient to reconstruct all other images, thanks to the rule (2.2)), we may consider the folding configurations as either short or long-edge configurations on the lattice, with constraints inherited from the rule (2.2). In both cases, we end up with statistical models with 4 edge variables, and only finitely many allowed vertices.

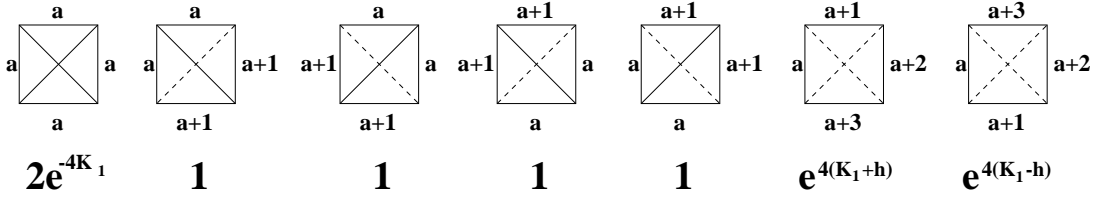


Fig. 2: The 28 possible face configurations of the rigid short edge model. The variable a may take any value mod 4. We have indicated the Boltzmann weights including a bending energy K_1 per short edge and a magnetic field h .

On long edges, the constraint (2.2) amounts to relating the four long edge images around each square face made of 4 triangles. Let us first introduce the orthogonal basis $(\vec{f}_1, \vec{f}_2) = (\vec{e}_1 + \vec{e}_2, \vec{e}_2 - \vec{e}_1)$ for long edge vectors, and label the edge values $\vec{f}_1, \vec{f}_2, -\vec{f}_1, -\vec{f}_2$ respectively by 0, 1, 2, 3. In terms of these values, the only edge configurations around a square face which are allowed by (2.2) are the 28 cases depicted in Fig.2. They correspond respectively to the following folding states of the inner short edges: all four folded (4), two folded along the same diagonal (16), none folded (8). In Fig.2, we have represented in dashed lines the unfolded short edges, and in solid lines the folded ones. Introducing a bending energy J_1 to distinguish between folded and unfolded short edges, we are led to weight the first case of Fig.2 by e^{-4K_1} , the next four by 1 and the two last ones by e^{4K_1} , where $K_1 = -J_1/kT$. To complete the definition of the model, we need to introduce

a suitable order parameter for the folding transition. This parameter should distinguish between flat and folded phases. Following [4], we introduce a fictitious magnetic field H , coupled to the normal vectors to the faces, defined in such a way that they all point up in a completely flat configuration of the lattice. The corresponding magnetization is the order parameter for the folding transition. Setting $h = -H/kT$, the two last face configurations of Fig.2 receive extra Boltzmann weights $e^{\pm 4h}$ respectively, as one of these two flat faces points up and the other points down. This model is studied in Sect.3 below.

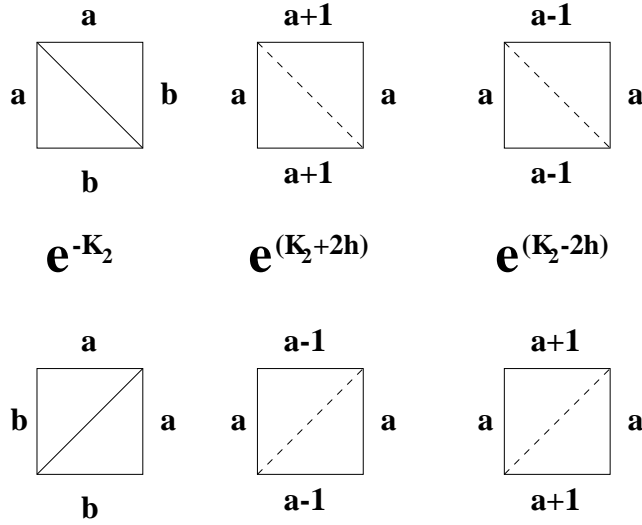


Fig. 3: The 32 possible face configurations of the rigid long edge model. The variables a, b may take any values mod 4, with $a \neq b \pmod{2}$. This gives 8 configurations for each of the first cases, and 4 for each of the second and third ones. We have indicated the Boltzmann weights including a bending energy K_2 and a magnetic field h .

On short edges, the constraint (2.2) implies first that the two short edges of each triangle must have perpendicular images. Using again a \mathbb{Z}_4 short edge variable reading respectively 0, 1, 2, 3 for the edge values $\vec{e}_1, \vec{e}_2, -\vec{e}_1, -\vec{e}_2$, this means that $a \neq b \pmod{2}$ for the two short edge values a, b of a given triangle. The constraint also relates the short edge images of any two triangles sharing a long edge as follows. If \vec{u}, \vec{v} stand for the short edge images of the first triangle, and \vec{u}', \vec{v}' the second, there are only two ways to accommodate $\vec{u} + \vec{v} = \vec{u}' + \vec{v}'$, namely $\vec{u}' = \vec{u}$ and $\vec{v}' = \vec{v}$, or $\vec{u}' = \vec{v}$ and $\vec{v}' = \vec{u}$. The corresponding configurations are depicted in Fig.3, for the two types of faces (according to the position of the long edge). In the first cases, the common long edge is folded (solid line), whereas in the second and third it is not (dashed line). Introducing a bending energy J_2 to distinguish between folded and unfolded long edges, we decide to weight the first

cases with a Boltzmann weight e^{-K_2} , and the second and third ones with a weight e^{K_2} , with $K_2 = -J_2/kT$. As before, we introduce a magnetic field H coupled to the normal vectors to the membrane. This results in an extra Boltzmann weight $e^{\pm 2h}$ for respectively the second and third cases of Fig.3, with a flat face respectively pointing up and down. This model is studied in Sect.4 below.

The general model including bending rigidity for both types of edges is studied in Sect.6. In all cases, we will construct a row-to-row transfer matrix T for rows of width $L = 1, 2, \dots$ and extract its largest eigenvalue, which dominates the partition function

$$Z = \text{Tr}(T^M) \sim \lambda_{max}^M \sim e^{LMf} \quad (2.3)$$

when L and M become large. This will lead to numerical estimates for the thermodynamic free energy f per site (note the change of sign and the absence of the usual $1/kT$ in the definition of f , for notational simplicity). All the transfer matrices we are dealing with are sparse due to the relatively short number of allowed face configurations, compared to the size of the matrices. We therefore use an efficient algorithm which codes the matrices as the list of their non-vanishing elements, together with their position, and then extracts the largest eigenvalue by repeated iteration on a given vector.

3. Rigid Short Edge Model

Including the abovementioned magnetic field $h = -H/kT$, the Boltzmann weights for the face configurations of Fig.2 read

$$w_1 = e^{-4K_1} \quad w_2 = w_3 = w_4 = w_5 = 1 \quad w_6 = e^{4K_1+4h}, \quad w_7 = e^{4K_1-4h} \quad (3.1)$$

Note that the effect of the magnetic field is to distinguish the configurations in which the normal vectors all point up (energy $-4H$) or all point down (energy $4H$), from all other cases, where there are as many up and down-pointing normal vectors.

For definiteness, let us denote by $w(a, b, c, d)$ the Boltzmann weight attached to a cyclic configuration (a, b, c, d) of edge variables, clockwise around the square face with a in the west position. The row-to-row transfer matrix of the model for a row of L square faces then reads

$$T_{a_1, \dots, a_L; a'_1, \dots, a'_L} = \sum_{b_1, \dots, b_{L+1} \in \mathbb{Z}_4} \prod_{i=1}^L w(b_i, a'_i, b_{i+1}, a_i) \quad (3.2)$$

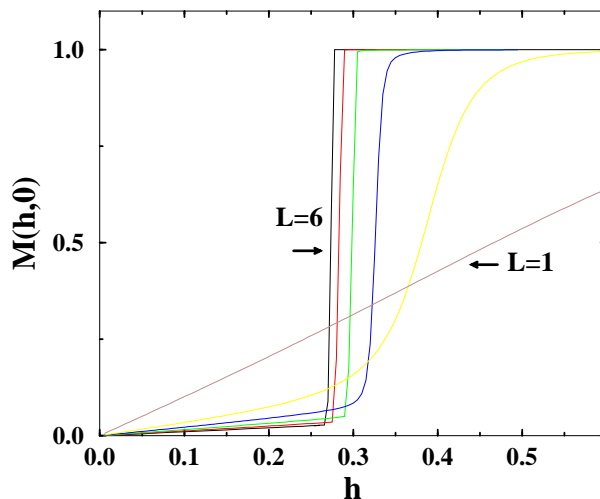


Fig. 4: Magnetization versus magnetic field for the rigid short edge model at $K_1 = 0$, for strips of width $L = 1, 2, \dots, 6$. We see clearly two phases: folded, with $M \rightarrow 0$, and flat, with $M = 1$. We expect the transition between the two to be discontinuous in the thermodynamic limit $L \rightarrow \infty$.

This matrix has size $4^L \times 4^L$ and is sparse, as there are only $\sim 7^L$ non-vanishing elements (given the west value, there are exactly 7 allowed face configurations). The numerical result of [4] for the entropy of folding $f = s_{SD} \simeq .230\dots$ is readily recovered for $K_1 = h = 0$.

We display in Fig.4 the magnetization $M = \partial_h f$ for various sizes $L = 1, 2, \dots, 6$ at $K_1 = 0$. Even for these finite values of L , we see a drastic jump in the magnetization at a value $h = h_{c,L}(K_1 = 0)$ of the magnetic field. Extrapolating these, we find that they tend to a limiting value $h_c(0) = .23\dots$ for large L . In the low- h phase, the magnetization has a small finite slope, which tends to 0 for large L . In the large- h phase, the magnetization is identically 1. We conclude that the system is reduced to two phases, a completely folded one for $h < h_c(0)$ and a completely flat one for $h > h_c(0)$. Note that $h_c(0) \simeq s_{SD}$.

This two-phase situation is observed for other values of K_1 in Fig.5, where we have represented the corresponding magnetizations as functions of h for $L = 6$. Like in [4], this leads us to formulate the hypothesis that, at least for small enough K_1 , there will always exist only two phases, folded and flat, with $M = 0$ and 1 respectively. Let $f_0(K_1)$ denote the free energy per triangle of the model in zero magnetic field. This is exactly the energy of the folded phase of our model, as the latter is insensitive to the magnetic field. Note that this phase is entropic, at least when $K_1 = 0$, where $f_0(0) = s_{SD} = .230\dots$ On the other hand, the completely flat phase consists of configurations made only of faces of the

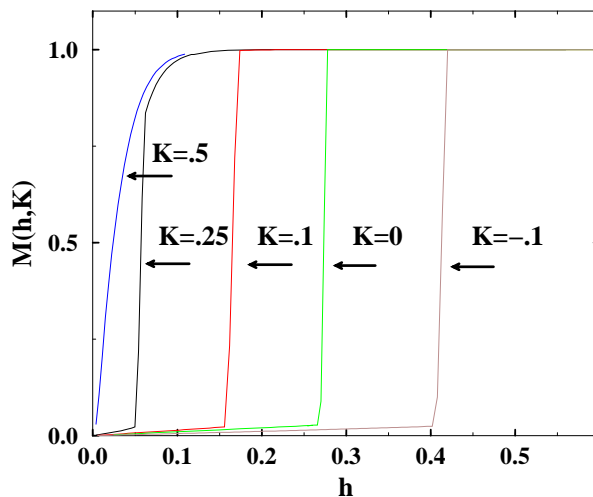


Fig. 5: The magnetization as a function of the magnetic field for strips of width $L = 6$, and various values of $K_1 = .5, .25, .1, 0, -.1$. A change of behavior is observed for $K_1 = .5$: there, we expect the folded phase to disappear in the thermodynamic limit.

form $(a, a + 1, a + 2, a - 1)$, with weight $w_4 = e^{4(K_1+h)}$, hence resulting in a thermodynamic energy $f_1(K_1, h) = K_1 + h$ per triangle. The critical field $h_c(K_1)$ is then defined by the equality of the two energies, namely

$$h_c(K_1) = f_0(K_1) - K_1 \quad (3.3)$$

Let $\lambda_{max}^{(L)}(K_1)$ denote the largest (Perron-Frobenius) eigenvalue of the transfer matrix T of (3.2). Taking $\phi_{0,L}(K_1) = \text{Log}(\lambda_{max}^{(L)}(K_1))/(4L)$ as a sequence of approximations for $f_0(K_1)$, the folded phase energy, is not very accurate, as it includes a generic two-fold degeneracy due to the invariance under reversal of all non-horizontal tangent vectors, i.e. a folding along the top or bottom horizontal line of the row (in which, in particular, the two face configurations $(a + 1, a + 2, a - 1, a)$ and $(a - 1, a + 2, a + 1, a)$ are exchanged). We should rather use

$$f_{0,L}(K_1) = \phi_{0,L}(K_1) - \frac{1}{4L} \text{Log } 2 \quad (3.4)$$

by explicitly dividing out the degeneracy. Although in principle equivalent to $\phi_{0,L}(K_1)$ in the thermodynamic limit, $f_{0,L}$ displays a much better convergence. Let us now turn to the finite L flat phase energy $f_{1,L}(K_1, h)$. The flat phase matrix elements of T are

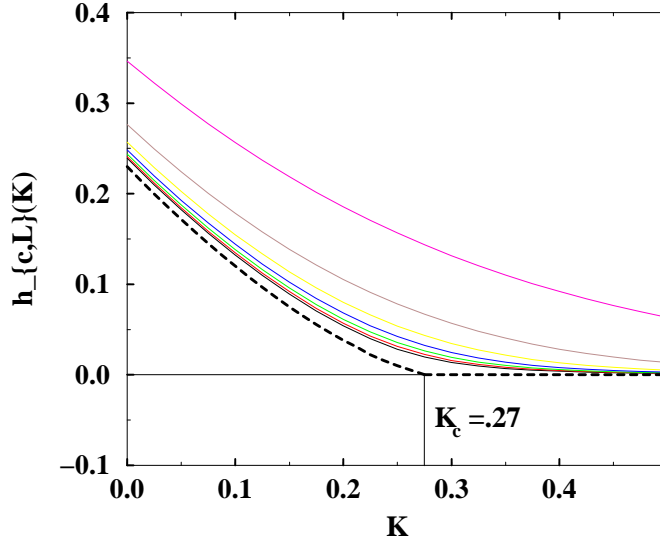


Fig. 6: The critical field $h_{c,L}(K)$ for $L=1,2,\dots,7$ (from top to bottom). We have represented in dashed line the extrapolated limiting curve for $L \rightarrow \infty$. It displays a transition at $K = K_{c1} \simeq .27$.

non-diagonal, and read $T_{a,a+2,a,a+2,\dots;a+2,a,a+2,a,\dots} = 2e^{4LK_1} \cosh(4Lh)$. They give the energy

$$f_{1,L}(K_1, h) = K_1 + h + \frac{1}{4L} \text{Log}(1 + e^{-8Lh}) \quad (3.5)$$

Due to the exponential character of the correction, the approximation to the critical field, $h_{c,L}(K_1) = f_{0,L}(K_1) - K_1$ is accurate, at least in the large h phase. We have represented in Fig.6 the critical field $h_{c,L}(K)$ as a function of K , for various values of L . These curves are extrapolated to the large L limiting curve represented in dashed line. This curve has also been obtained by the extrapolation of another sequence of approximations, namely

$$h_{c,L/L+1}(K) = \frac{1}{4} \text{Log} \left(\frac{\lambda_{max}^{(L+1)}(K)}{\lambda_{max}^{(L)}(K)} \right) - K \quad (3.6)$$

for $L = 1, 2, \dots, 6$, with an excellent agreement. We observe the existence of a finite value $K_{c1} = .27$ of K_1 beyond which h_c vanishes identically.

4. Rigid Long Edge Model

Including the magnetic field $h = -H/kT$, the Boltzmann weights of the configurations of Fig.3 read respectively

$$w_1 = e^{-K_2} \quad w_2 = e^{K_2+2h} \quad w_3 = e^{K_2-2h} \quad (4.1)$$

As before, let $w(a, b, c, d)$ stand for the Boltzmann weight of the configuration (a, b, c, d) around the face, clockwise with a in the western position. By a slight abuse of notation, we will use the same letters to denote the Boltzmann weights, transfer matrix, energy, etc... of the present model as those used for the Rigid Short Edge model of previous section.

With these definitions, the transfer matrix for a row of width L reads

$$T_{a_1, \dots, a_L; a'_1, \dots, a'_L}(h, K) = \sum_{b_i, c_i, d_i \in \mathbb{Z}_4} \prod_{i=1}^L w(b_i, c_i, b_{i+1}, a_i) w(d_i, a'_i, d_{i+1}, c_i) \quad (4.2)$$

Indeed, because of the alternance of the long edge between first and second diagonal in the short square faces, we must consider two rows of square faces, with a total of $4L$ triangles. Let us note however that $T = U(h, K)U^t(-h, K)$, where $U(h, K)$ is the transfer matrix for the first row, with entries

$$U_{a_1, \dots, a_L; a'_1, \dots, a'_L}(h, K) = \sum_{b_i \in \mathbb{Z}_4} \prod_{i=1}^L w(b_i, a'_i, b_{i+1}, a_i) \quad (4.3)$$

Indeed, upon transposition, the picture for U is reflected wrt a horizontal line, hence the inner long edge on each face switches to the other diagonal, which amounts to a change $h \rightarrow -h$ according to Fig.3.

n	λ_{max}	ν_n
1	4.000000	1.22891
2	6.040895	1.23758
3	9.252396	1.24610
4	14.36690	1.24926
5	22.42177	1.25212
6	35.15328	1.25351
7	55.23640	1.25482
8	86.97476	1.25558
9	137.1155	1.25631
10	216.4118	

Table I: Numerical results for the maximum eigenvalue of the square root of the transfer matrix of the rigid long edge model with free boundary conditions.

We have represented the size n of the row, the largest eigenvalue and the ratio $\nu_n = (\lambda_{n+1}/\lambda_n)^{1/2}$, which converges to the partition function per triangle.

This remark makes the numerical study much simpler, as the extraction of the largest eigenvalue of T is done by iterating the action of U and U^t in alternance on a given vector. Again, U is sparse, with a number of non-zero elements $\sim 2^L$ much smaller than its size 4^L . As an application, we list in Table I the largest eigenvalue of the matrix $\sqrt{T} = \sqrt{UU^t}$ for $K_2 = h = 0$, and for $L = 1, 2, \dots, 10$. This is in agreement with the estimate for the partition function per triangle $z_{SD} = 1.258\dots$ of [5].

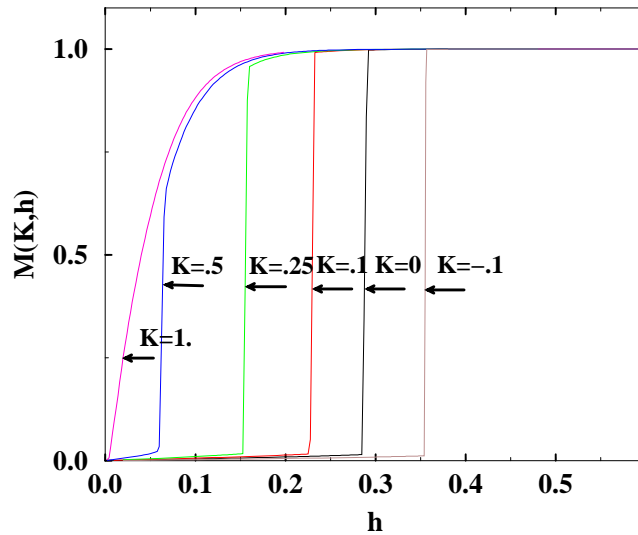


Fig. 7: Magnetization versus magnetic field for strips of width $L = 7$ in the rigid long edge model, for various values of K . We note the existence of two phases with respectively $M = 0$ (folded) and $M = 1$ (flat).

The two-phase hypothesis of the previous section is confirmed here in Fig.7, where we have represented the magnetization as a function of h for $L = 7$ and various values of K_2 . An analogous reasoning leads to the determination of the critical magnetic field $h_c(K_2) = f_0(K_2) - \frac{K_2}{2}$, obtained by equating the energies of the folded and flat phases. Here the flat phase is made of only the face configuration $(a, a + 1, a, a + 1)$, hence an energy of $f_1(K_2, h) = (2L(K_2 + 2h))/(4L) = \frac{K_2}{2} + h$.

For strips of finite size L however, the folded phase energy reads

$$f_{0,L}(K_2) = \frac{1}{4L} \text{Log} \lambda_{\max}^{(L)}(K_2) - \frac{1}{4L} \text{Log} 4 \quad (4.4)$$

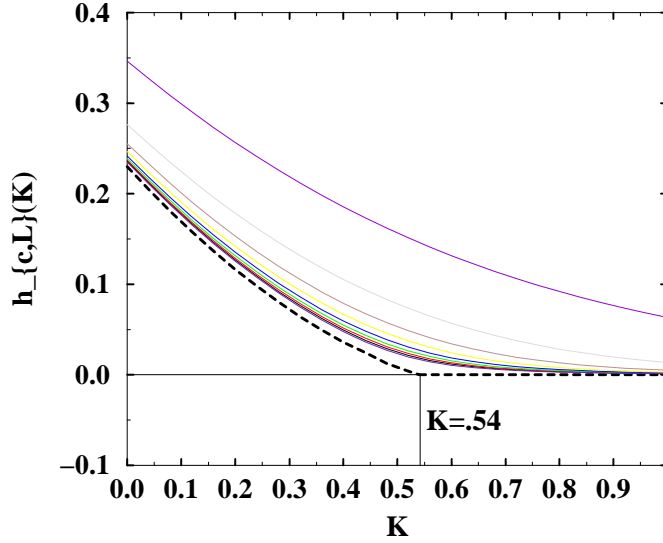


Fig. 8: The critical fields $h_{c,L}(K)$ for $L = 1, 2, \dots, 9$. We have represented the extrapolated large L limit in thick dashed line. It displays a transition at the critical value $K_{c,2} \simeq .54$.

where $\lambda_{max}^{(L)}(K_2)$ is the largest (Perron-Frobenius) eigenvalue of the transfer matrix T (4.2) for a row of $2 \times L$ squares. Note the subtraction of the $4 = 2 \times 2$ times degeneracy under the previously mentioned reversal of non-horizontal tangent vectors, in which in particular $(a+1, a, a+1, a) \leftrightarrow (a-1, a, a-1, a)$. On the other hand, the flat phase energy corresponds to the diagonal matrix elements $T_{a,a,a,\dots;a,a,a,\dots}$, $a \in \mathbb{Z}_4$, with only face configurations of the type (b, a, b, a) and $b \neq a \pmod{2}$. This gives four identical diagonal blocks, with eigenvalue

$$\lambda_{max}^{(L)}(K_2, h) = 2e^{2LK_2} \cosh(4Lh) \quad (4.5)$$

and the energy

$$f_{1,L}(K_2, h) = \frac{K_2}{2} + h + \frac{1}{4L} \text{Log}(1 + e^{-8Lh}) \quad (4.6)$$

Neglecting the exponential correction, the equality between (4.6) and (4.4) yields the finite size critical field

$$h_{c,L}(K_2) = f_{0,L}(K_2) - \frac{K_2}{2} \quad (4.7)$$

which we have represented for various values of L in Fig.8. We observe an excellent convergence of the quantity $h_{c,L}(K_2)$, and a particular value $K_{c,2} \simeq .54$ of K_2 beyond which the critical field h_c vanishes identically, hence only the flat phase survives. Note that we get $K_{c,2} \simeq 2K_{c,1}$.

5. Continuous Transitions for $K < 0$

As observed in [4] in the case of the triangular lattice folding, both short and long rigid edge models undergo continuous phase transitions for some negative critical values $K_{*,1}$ and $K_{*,2}$ of K . In terms of our initial setting, these are anti-ferromagnetic transitions. However, they take place in the entropic (folded) phase of both models, in which local excitations can be formed, as explained in [5].

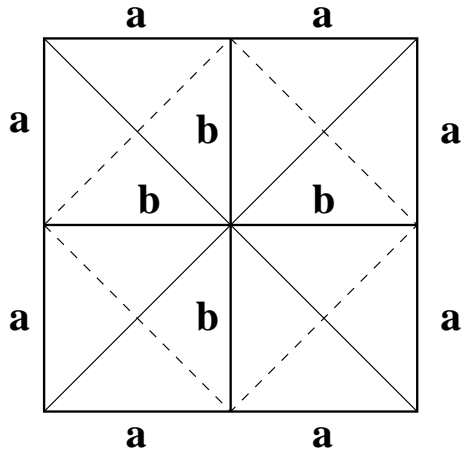


Fig. 9: A local excitation of one of the anti-ferromagnetic (completely folded) groundstates of the rigid short edge model. The unfolded short edges are represented in dashed line. All others remain folded.

More precisely, in the rigid short edge model, starting from one of the (completely folded) anti-ferromagnetic groundstates, in which all the short edges are completely folded, hence where all long edges take the same value a , we can unfold a square of 8 short edges, as shown in Fig.9. This is a local excitation of the anti-ferromagnetic groundstate, which receives a relative Boltzmann weight $2e^{-16K_1}$, including the effect of unfolded edges and the free choice of the two orientations $b = a \pm 1$ of the new tangent vectors. Note that we have not specified the folding state of the long edges, which results in a non-vanishing entropy of the model. Such local excitations can be combined so as to form any loops of unfolded short edges (with the constraint that these edges can only be unfolded by parallel pairs within each square of long edges).

In the rigid long edge model, similar excitations of the (completely folded) anti-ferromagnetic groundstate may occur. They correspond to unfolding four long edges forming a square, as shown in Fig.10. This excitation receives a relative Boltzmann weight $2e^{-8K_2}$. Again, these excitations may be combined into any loop of unfolded long edges.

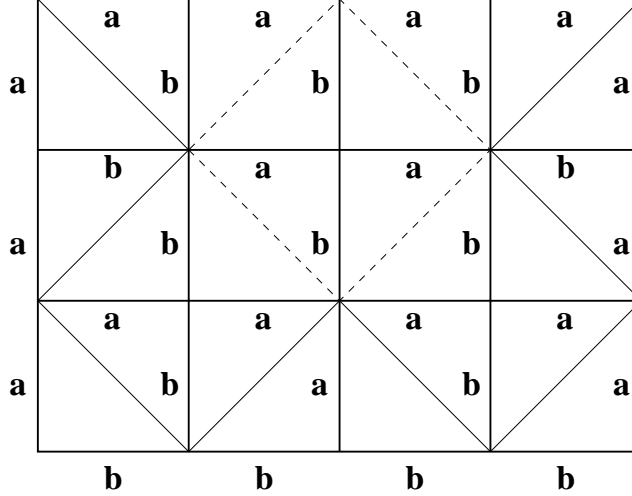


Fig. 10: A local excitation of one of the anti-ferromagnetic (completely folded) groundstates of the rigid long edge model (with $a \neq b \pmod 2$). The four dashed long edges have been unfolded in the process, while all others remain folded.

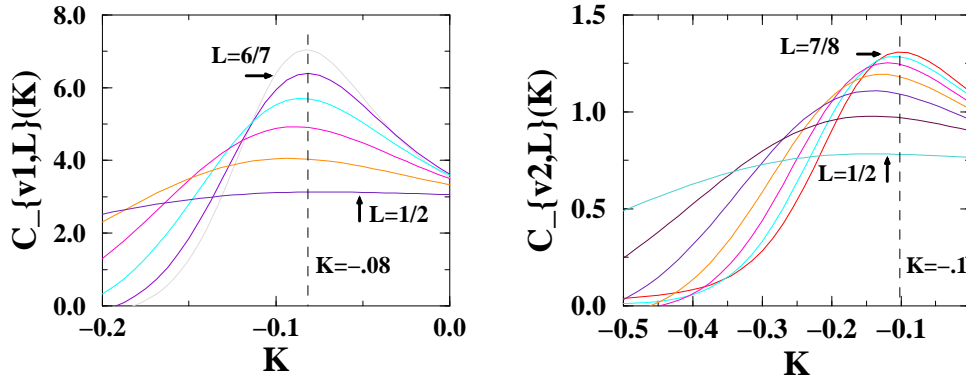


Fig. 11: Specific heat vs K for the rigid short (1) and long (2) edge models. The pairs $L/L + 1$ used to evaluate the curves are indicated. Both models display a continuous transition. The critical values of K are estimated to be $K_{*,1} = -.08$ and $K_{*,2} = -.1$.

In both cases, the resulting loop model is naturally expected to undergo a phase transition of the Ising type, when $K_1, K_2 < 0$ cross some critical values. To check this, we have represented in Fig.11 for $L = 1, 2, \dots, 6$ or 7 the specific heats $C_{v1,L}(K_1) = \partial_{K_1}^2 \varphi_{1,L}(K_1)$ and $C_{v2,L}(K_2) = \partial_{K_2}^2 \varphi_{2,L}(K_2)$, where the approximations to the free energy are taken to be

$$\varphi_{i,L}(K_i) = \frac{1}{4} \text{Log} \left(\frac{\lambda_{max}^{(L+1)}(K_i)}{\lambda_{max}^{(L)}(K_i)} \right) \quad (5.1)$$

We observe the typical growth of the maximum of the specific heat with L , which points to critical values of K reading respectively $K_{*,1} = -.08$ and $K_{*,2} = -.1$. Using the graphs of Fig.11, we have also obtained estimates for the thermal critical exponents α_i such that in the thermodynamic limit $C_{vi}(K_i) \simeq |K_i - K_{*,i}|^{-\alpha_i}$, with the results $\alpha_1 \simeq .2$ and $\alpha_2 \simeq .25$.

6. General Phase Diagram

Let us now address the general rigid (long and short) edge model for the square-diagonal lattice folding problem. This is simply a combination of the two models of Sects.3 and 4, where the long and short edges receive the Boltzmann weights $e^{\pm K_1}$ (short) and $e^{\pm K_2}$ (long) for unfolded (+) and folded (-) states of the edge.

In view of the results of Sects.3,4 and 5, we expect a very interesting phase diagram for this general model, in which both first order and continuous transition can be found.

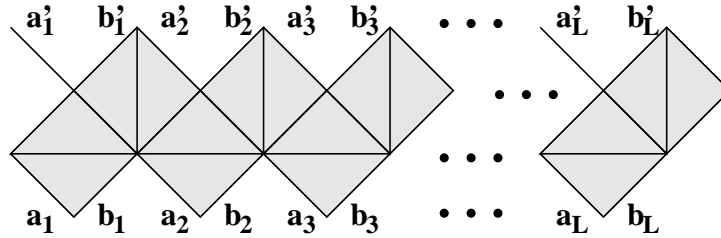


Fig. 12: The row-to-row transfer matrix T for the general rigid long and short edge model. T acts by transferring a zig-zag row $\{(a_1, b_1), (a_2, b_2), \dots, (a_L, b_L)\}$ of pairs of adjacent short edges to the nearest vertical translate.

The transfer matrix T of the general model reads as follows. We consider a row of $4L$ triangles, as shown in Fig.12, which transfers a zig-zag line of $2L$ short edges to the nearest translate above it. The short edges in a line naturally go by pairs of adjacent edges sharing the same triangle, with a total of 8 possible images, $a, b \in \mathbb{Z}_4$, with $a \neq b \pmod{2}$, expressing the fact that the corresponding tangent vectors are orthogonal. Hence we may view T as a $8^L \times 8^L$ matrix acting in the space of pairs of adjacent short edges along a zig-zag line of $2L$ edges.

The matrix T is made of L cells, expressing the various Boltzmann weights and constraints on the short and long inner edges. We distinguish three pieces, according to Fig.13,

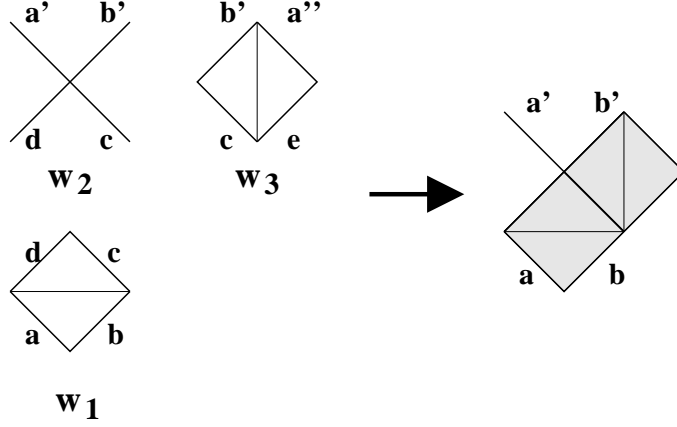


Fig. 13: The transfer matrix of the rigid long and short edge model is made of three elementary Boltzmann weights w_1, w_2, w_3 corresponding to the arrangements of inner short edges $c, d, e \in \mathbb{Z}_4$, with $c \neq d \pmod{2}$, and outer short edges $a, b, a', b', a'' \in \mathbb{Z}_4$, with $a \neq b \pmod{2}, a' \neq b' \pmod{2}$.

with the Boltzmann weights

$$\begin{aligned}
w_1(a, b, c, d) &= e^{K_2} \delta_{a,c} \delta_{b,d} + e^{-K_2} \delta_{a,d} \delta_{b,c} \\
w_2(a', b', c, d) &= (e^{2K_1} \delta_{a',c+2} + e^{-2K_1} \delta_{a',c}) (e^{2K_1} \delta_{b',d+2} + e^{-2K_1} \delta_{b',d}) \\
w_3(b', a'', e, c) &= e^{K_2} \delta_{b',e} \delta_{a'',c} + e^{-K_2} \delta_{a'',b'} \delta_{e,c}
\end{aligned} \tag{6.1}$$

where $\delta_{p,q} = 1$ if $p = q \pmod{4}$, 0 otherwise. The transfer matrix elements then read

$$\begin{aligned}
T_{\{a_i, b_i\}; \{a'_i, b'_i\}} &= \\
\sum_{\substack{c_i, d_i, a'_{L+1}, d_{L+1} \in \mathbb{Z}_4 \\ i=1, 2, \dots, L}} \prod_{i=1}^L w_1(a_i, b_i, c_i, d_i) w_2(a'_i, b'_i, c_i, d_i) w_3(b'_i, a'_{i+1}, d_{i+1}, c_i)
\end{aligned} \tag{6.2}$$

Inspecting (6.1), we see that T has $\sim 16^L$ non-vanishing entries, for a size $8^L \times 8^L$, hence is a sparse matrix. But the size is of course much more limiting than in the cases of Sects.3 and 4.

The transition curves we are looking for are characterized numerically, for finite size L of the transfer matrix, by a growing peak of the specific heat. To identify those in the K_1, K_2 plane, we have located the maxima of the specific heat along lines through the origin. More precisely, taking $K_1 = K \cos(\theta)$ and $K_2 = K \sin(\theta)$, we have taken a discrete set of angles $\theta \in [-\pi/2, \pi/2)$, and represented the maxima of the specific heat

$$C_{v,L}(K) = \partial_K^2 \frac{1}{4L} \text{Log} \left(\lambda_{max}^{(L)}(K \cos(\theta), K \sin(\theta)) \right) \tag{6.3}$$

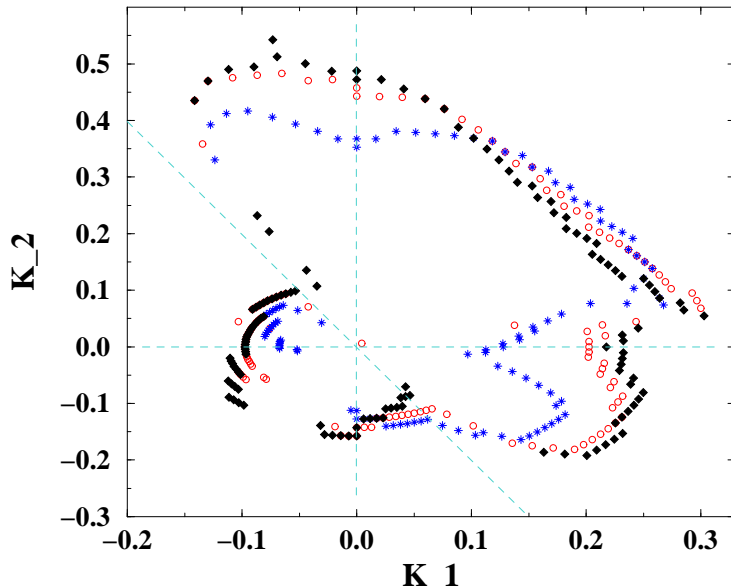


Fig. 14: Maxima of the specific heat $C_{v,L}(K_1, K_2)$ for $L = 2$ (stars), $L = 3$ (circles) and $L = 4$ (diamonds), in the (K_1, K_2) plane. We have represented the axes as well as the line $K_2 = -2K_1$ in dashed lines. The latter appears to be the separation between the continuous (anti-ferromagnetic) transition curve and the first order (ferromagnetic) one.

where $\lambda_{max}^{(L)}(K_1, K_2)$ denotes the maximum (Perron-Frobenius) eigenvalue of the transfer matrix T defined above, for a strip of width L . The results for $L = 2, 3, 4$ and $\theta = k\pi/(2m)$, $k = -m, -m + 1, \dots, m - 2, m - 1$, $m = 35$, are displayed in Fig.14.

Note that the separation between the two transition curves, continuous anti-ferromagnetic (negative K 's) and first order ferromagnetic (positive K 's) appears to lie precisely on the line $K_2 = -2K_1$. This should not be too much of a surprise, if we note that there are exactly twice as many short edges as long ones in the square-diagonal lattice. The anti-ferromagnetic and ferromagnetic bending energies are precisely balanced along the line $K_2 = -2K_1$. As a check of the crossing between the two curves, we have represented the specific heat $C_{v,4}(K_1, -2K_1)$ for $L = 4$ in Fig.15. We see clearly the four critical points, two of which lie on the continuous transition curve, and two on the first order one.

We are naturally led to conjecture the thermodynamic picture of Fig.16 when $L \rightarrow \infty$, with two transition curves, continuous (anti-ferromagnetic) in dashed line, and first order (ferromagnetic) in solid line. Outside of the solid curve, and above the line $K_2 = -2K_1$,

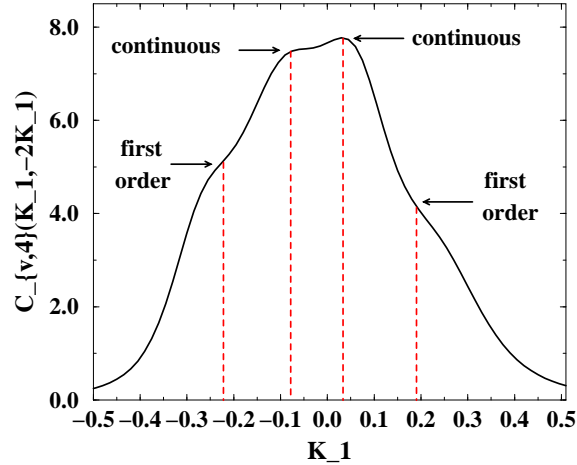


Fig. 15: The specific heat $C_{v,4}(K_1, -2K_1)$ for $L = 4$, along the crossing line $K_2 = -2K_1$. We have indicated the transition points (or remnants thereof).

the model is always in the completely flat phase with magnetization $M = 1$ if $h \rightarrow 0^+$ and $M = -1$ if $h \rightarrow 0^-$. Outside of the dashed curve, and below the line $K_2 = -2K_1$, the model is in a completely folded phase, with possibly some unfolded loops of edges. The staggered (anti-ferromagnetic) magnetization M_{st} corresponding to a staggered magnetic field h_{st} (taking alternating values $\pm h_{st}$ on adjacent triangles) is a function of the K 's tending to 1 if $h_{st} \rightarrow 0^+$ and -1 if $h_{st} \rightarrow 0^-$ for large negative K 's. The dashed curve corresponds to the vanishing of the staggered magnetization, which becomes identically zero inside the curve. So the region inside both curves corresponds to both magnetizations equal to zero: we can think of it as a partially folded (or unfolded) phase.

To fully illustrate the ferromagnetic transition, we have represented schematically (most of the curves are represented as lines) in Fig.17 the surface $h = h_c(K_1, K_2)$ of the critical magnetic field beyond which the membrane is in the completely flat phase, and below which it is folded. This surface is singular along the plane $K_2 = -2K_1$: $h(K_1, K_2)$ has a jump discontinuity from one of its sides to the other, except at $K_1 = K_2 = 0$. The corresponding point $h = h_{SD} = h_c(0, 0)$ is a conic singularity of the surface.

Acknowledgements

This work was partially supported by NSF grant PHY-9722060.

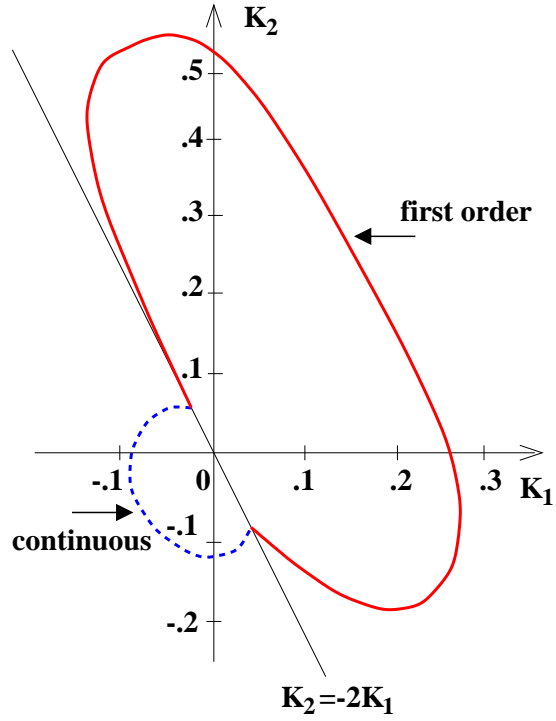


Fig. 16: The extrapolated critical lines of the short and long rigid edge model in the plane (K_1, K_2) . The solid line curve represents the first order (ferromagnetic) critical line, involving in particular values $K_1 > 0$ and $K_2 > 0$. Large positive K_1 's and K_2 's correspond to ferromagnetic order, i.e. the completely flat phase. The dashed line curve represents the continuous (anti-ferromagnetic) Ising-like transition line, involving in particular values $K_1 < 0$ and $K_2 < 0$. Large negative K_1 's and K_2 's correspond to anti-ferromagnetic order, hence a completely folded phase.

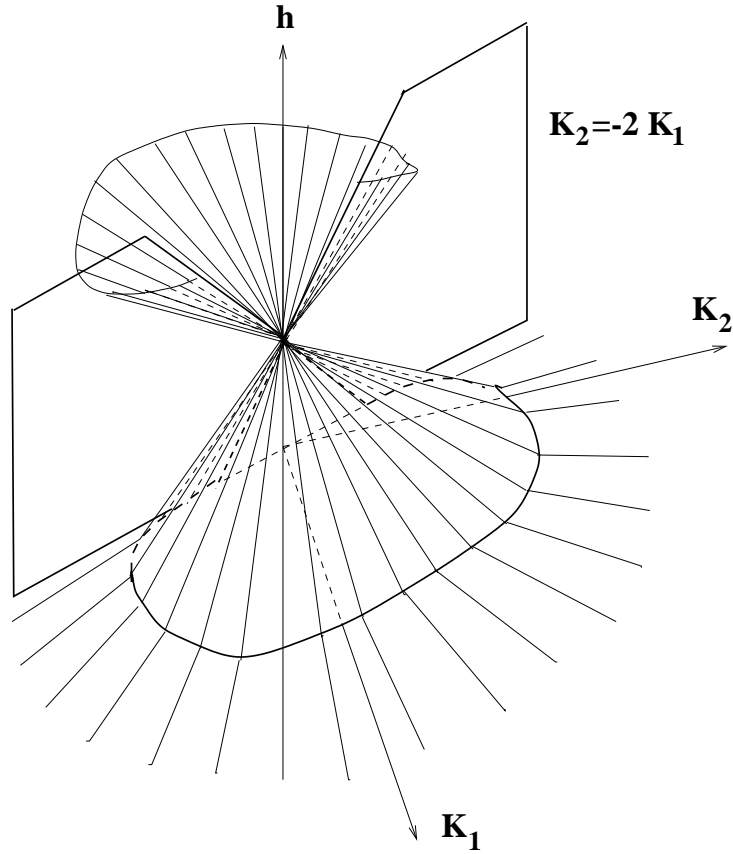


Fig. 17: A rough sketch of the surface $h = h_c(K_1, K_2)$ for the critical magnetic field separating the flat and folded phases of the membrane. This surface coincides with the plane $h = 0$ outside of the transition curve and in the domain $K_2 > -2K_1$. Note the conic singularity at the point $(0, 0, h = s_{SD})$, and the jump singularities along the plane $K_2 = -2K_1$.

References

- [1] P. Di Francesco, O. Golinelli and E. Guitter, *Meander, Folding and Arch Configurations*, Mathl. Comput. Modelling, Vol. **26**, No.8-10 (1997) 97-147, *Meanders and the Temperley-Lieb Algebra*, Commun. Math. Phys. **186** (1997), 1-59 and *Meanders: a direct enumeration approach*, Nucl. Phys. **B482[FS]** (1996), 497-535; P. Di Francesco, *Meander Determinants*, Commun. Math. Phys. **191** (1998) 543-583.
- [2] Y. Kantor and M.V. Jarić, Europhys. Lett. **11** (1990) 157.
- [3] P. Di Francesco and E. Guitter *Entropy of Folding of the Triangular Lattice*, Europhys. Lett. **26** (1994) 455.
- [4] P. Di Francesco and E. Guitter *Folding Transition of the Triangular Lattice*, Phys. Rev. **E50** (1994) 4418-4426.
- [5] P. Di Francesco *Folding the Square-Diagonal Lattice*, preprint UNC-CH-MATH 98/1, cond-mat/9803051, accepted for publication in Nucl. Phys. **B** (1998).